Colloids and Surfaces B: Biointerfaces 161 (2018) 588–596

Contents lists available at ScienceDirect

Colloids and Surfaces B: Biointerfaces

journal homepage: www.elsevier.com/locate/colsurfb

Full Length Article

# Liposomally formulated phospholipid-conjugated novel near-infrared fluorescence probe for particle size effect on cellular uptake and biodistribution in vivo

Jing Xing[a,b], Dong Liu[a,b], Gaoxin Zhou[a,b], Yuan Li[a,b], Peng Wang[c], Ke Hu[d], Ning Gu[a,b,*], Min Ji[a,b,*]

[a] School of Biological Science & Medical Engineering, Southeast University, Nanjing 210096, China
[b] School of Biological Science and Medical Engineering & Collaborative Innovation Center of Suzhou Nano Science and Technology, Southeast University, Suzhou 215123, China
[c] Department of Biomedical Engineering, School of Engineering, China Pharmaceutical University, Nanjing 210009, China
[d] Key Laboratory of Clinical and Medical Engineering, Department of Biomedical Engineering, School of Basic Medical Science, Nanjing Medical University, Nanjing 210000, China

ARTICLE INFO

*Article history:*
Available online 15 November 2017

*Keywords:*
Phospholipid-conjugated
Near-infrared fluorescence probe
Lipid based nanoparticles
Particle size
Cellular uptake
Biodistribution

ABSTRACT

Lipid based nanoparticles (LBNs) with excellent biocompatibility and versatility have received much attention from the drug delivery community recently. A detailed understanding of in vitro and vivo fate of LBNs is important for developing different types of LBNs with improved selectivity and low cytotoxicity. We developed a novel near-infrared (NIR) probe with high fluorescence, designated as DSPE-ir623 (iDSPE). Then, we prepared iDSPE-embeded liposomes (iLPs) with two different hydrodynamic sizes (~100 nm and ~400 nm) to evaluate the effect of particle size on cellular uptake and biodistribution of nanoliposomes in vivo. These iLPs were proved to exhibit good monodispersity, excellent fluorescence and stability. In vitro cell uptake tests demonstrated that iLPs-1 (~100 nm) were taken up more by HT-29 cells than iLPs-2 (~400 nm). Notably, the fluorescence of iLPs can be employed for real-time monitoring of the subcellular locating and its metabolic distribution in vivo. Near-infrared imaging in vivo illustrated that iLPs-1 was mainly accumulated in the tumor tissues, while iLPs-2 was accumulated in liver and spleen. The results indicated that the size of iLPs play an important role in the regulation of intracellular trafficking and biodistribution of liposomes, which also provide a new insight into the development of more effective LBNs. Hence, iDSPE might be a promising tool for the reliable tracing of different types of LBNs.



## 1. Introduction

Drug delivery systems aim to deliver drugs to their sites of action within an organism, with the goal of achieving a therapeutic outcome. During the few decades, nanoparticles as drug delivery system has gained an unprecedented popularity, due to its characteristic sustained drug release behavior, high drug loading capacity, high solubility of drug, low toxicity and good biocompatibility property [1–5]. Among various nanoparticles, LBNs have been widely studied in both research and industry [6,7]. LBNs have been widely used for delivering drugs, such as anticancer and antibacterial agents, imaging and probing agents, peptide hormones, proteins, enzymes, vaccines, and genetic material [8–12]. The in vivo fate of LBNs is essentially determined by the properties of their lipid compositions, particle size, and surface decoration [13–16]. Several studies have shown the improvement of oral absorption was mainly due to the permeation of LBNs as integral particles across intestinal epithelia [17]. While other researches showed that LBNs transformed into mixed micelles after lipolysis resulted in enhancing absorbability [13]. The underlying mechanisms of lipid based drug delivery systems are controversial for several years. In order to comprehend the accurate identification of integral LBNs in vivo and explore the fate of LBNs in vivo, recent studies have focused on the in vivo pharmacokinetics and biodistribution of LBNs using fluorescent probes for molecular imaging [18,19]. However, fluorescent probes can easily escape from the NP

DOI of original article: http://dx.doi.org/10.1016/j.colsurfb.2017.09.026.
* Corresponding authors at: School of Biological Science & Medical Engineering, Southeast University, Nanjing 210096, China
*E-mail addresses:* guning@seu.edu.cn (N. Gu), jimin@seu.edu.cn (M. Ji).

https://doi.org/10.1016/j.colsurfb.2017.11.033
0927-7765/

matrix but still retain the same fluorescent patterns. If the attached dye moiety is desorbed, released or removed in biological fluids, the tracing of fluorescence mislead the location of nanoparticles [20]. For quantitative and qualitative cellular and in vivo studies, the reliable tracing of LBNs is critical. To avoid these concerns, we have rationally designed and synthesized a novel near-infrared (NIR) probe for the tracing of LBNs with high fluorescence, designated as iDSPE, in which one indocyanine green (ICG) derivative ir623 was covalently conjugated with a phospholipid moiety, 1, 2-distearoyl-sn-glycero-3-phosphoethanolamine (DSPE). In general, the size of liposomes influences the pharmacokinetics and biodistribution [21,22]. Only liposomes with small particular size (≤100–150 nm) are able to exit or enter fenestrated vessels in the tumor microenvironment because of enhanced permeability and retention (EPR) effect [21,23,24]. In contrast, liposomes greater than 100–150 nm are often taken up by phagocytes or remain in the tissues for an extended time. The majority of phagocytes with liposomes accumulate in the liver and spleen for eventual elimination [25].

In this study, we developed iDSPE-embeded liposomes (iLPs) with two different hydrodynamic sizes (∼100 nm and ∼400 nm) to validate the effect of particle size on cellular uptake and biodistribution of nanoliposomes in vivo. Their physiochemical characters were systematically evaluated. In addition, iLPs with different sizes were subjected to HT-29 cell line to investigate their biocompatibility and size-dependent cellular uptake. Furthermore, in vivo metabolic distribution and accumulation were directly observed utilizing the NIR fluorescence of ir623. Overall, these studies suggest that vesicle size indeed affects cellular uptake and biodistribution of nanoliposomes in vivo. The novel near-infrared (NIR) probe, iDSPE developed for tracing of liposome may be easily extended to other lipid based nanoparticles (LBNs). It can be good models for studies try to comprehend the accurate identification of LBNs in vivo and explore the in vivo fate of LBNs.

## 2. Materials and methods

### 2.1. Materials and instruments

Chloroform and methanol were purchased from Shanghai Chemical Reagent Company. 1, 2-distearoyl-sn-glycero-3-phosphoethanolamine-N-[methoxy (polyethylene glycol)] (DSPE-PEG2000, 99%) was acquired from Southeast Pharmaceuticals Co. (Soochow, China). 2, 3, 3-Trimethylindolenine-5-sulfonic acid, *p*-methylbenzyl bromide, 2-chloro-1-formyl-3-hydroxymethylenecyclohexene, and ICG were purchased from Sigma-Aldrich (Shanghai).

$^1$H NMR were recorded on AVANCE AV-300 NMR spectrometer (Bruker, Switzerland). HRMS spectra was obtained on Q-TOF mass analyser (Agilent, USA). Fluorescence spectra were recorded on F4600 spectrofluorometer (Hitachi, Japan). Fluorescent images were obtained using Axiovert 200 fluorescence microscope (Zesis, Germany). The morphology of liposomes samples was observed by transmission electron microscopy (JEOL, Japan). Size distribution and zeta potential were acquired using a Nano-ZS 90 Nanosizer (Malvern, UK). NIR fluorescence in vivo imaging was carried out by IVIS Spectrum (Caliper Life Science, USA).

### 2.2. Chemical synthesis

#### 2.2.1. Synthesis of ir623

2, 3, 3-trimethylindolenine-5-sulfonic acid (1.24 g, 4.47 mmol) and 3-fluorobenzyl bromide (0.1 g, 5.81 mmol) were dissolved in 12 mL toluene. The solution was stirred under argon for 14 h at 90 °C. Vacuum filtration was performed to isolate the resulting precipitate and obtain a crude solid that was recrystallized to yield compound 3, which is a pink solid (1.31 g, yield 84.4%). Next, compound 3, 1- benzyl fluoride −2,3,3- three methyl −3H- indole −5- sulfonic acid (0.96 g, 2.76 mmol), compound 4, 2-chloro-1-formyl-3-hydroxymethylenecyclohexene (0.16 g, 0.95 mmol), and anhydrous sodium acetate (0.23 g, 2.76 mmol) were dissolved in 20 mL acetic anhydride. The solution was stirred under argon for 1 h at 75 °C. The resulting solution was added into the methyl *tert*-butyl ether to yield a crude solid. The crude residue was purified via column chromatography on silica gel using dichlormethane/methanol (10:1, $R_f$ = 0.30), which yielded compound 5 ir790 (380 mg, 33.1%) as emerald solid. The purified ir790 was characterized by NMR spectroscopy and mass spectrometry. Analysis of the data shows that ir790 was successfully prepared. $^1$H NMR (400 MHz,DMSO-*d*6):δ (ppm) = 1.73 (s, 14H), 2.54–2.57(t, *J* = 4 Hz,4H), 5.50(s,4H), 6.36–6.40(d,14 Hz,2H), 7.02–7.04(d,*J* = 8 Hz,2H), 7.14–7.19(m,4H), 7.33–7.35(d,*J* = 8.4 Hz,2 h), 7.38–7.44(m,4H), 7.625–7.629(d,*J* = 1.6 Hz,1H), 7.646–7.650(d,*J* = 1.6 Hz,1H), 7.85(s,2H),8.23–8.26(d,*J* = 14 Hz,2H); TOF-MS *m*/*z*: 829.3 $[M-H]^-$

Compound 5 ir790 (0.50 g, 0.60 mmol), and compound 6, 4- methyl benzoic acid (0.10 g, 0.66 mmol), and compound 7, N, *N*-diisopropylethylamine (93.3 mg, 0.72 mmol) were dissolved in 10 mL N, N-Dimethylformamide (DMF). The solution was stirred under argon for 6 h at 80 °C. The resulting solution was added into 200 mL methyl *tert*-butyl ether to yield a crude blue solid. The crude residue was purified via column chromatography on silica gel using dichlormethane/methanol (6:1, $R_f$ = 0.40), which yielded compound 8 ir623 (420 mg, 73.8%) as blue solid. $^1$H NMR (400 MHz, DMSO-*d6*): δ(ppm) = 1.31(s,14H,), 2.34(m,4H), 4.93(s,2H), 5.20(s,4H), 5.08(m,2H), 7.01–7.08(m,8H), 7.40–7.46(m,10H), 8.07(s,2H), 9.50(s,1H); TOF-MS *m*/*z*: 944.4 $[M]^-$, 472.2 $[(M-H)/2]^{-1}$

#### 2.2.2. Synthesis of DSPE-ir623 (iDSPE)

Briefly, ir623 (50 mg, 0.0528 mmol) was firstly activated in anhydrous DMF by NHS (24.3 mg, 0.2114 mmol) and DCC (21.81 mg, 0.1057 mmol) overnight at room temperature in dark. After filtered off the dicyclohexylurea (DCU) by-product, the resulting solution was added into the methyl *tert*-butyl ether to yield a crude solid. Then, the crude residue was purified via column chromatography on silica gel using dichlormethane/methanol (12:1), which yielded ir623-NHS (40 mg, 72.6%) as navy-blue solid. The intermediate product ir623-NHS was confirmed by thin layer chromatography (acetone: ethyl alcohol = 3: 2, $R_f$ = 0.85). The two blue spots from the intermediate product on the left column represent the unreacted ir623 (bottom spot) and the product ir623-NHS (top spot). The purified ir623-NHS was characterized by mass spectrometry, TOF-MS *m*/*z*: 1043.2 [M + H].

Afterward, DSPE (53.8 mg, 71.9 μmol) was added to a solution of TEA (48.5 mg, 0.479 mmol) in hot $CHCl_3$ (6 mL). Then the solution was mixed with ir623-NHS (50 mg, 0.0479 mmol) dissolved in DMSO (6 mL) stirred in dark for 20 h at room temperature. After addition of methyl *tert*-butyl ether (50 mL) to crystallize the product, the crude residue was purified via column chromatography on silica gel using dichlormethane/methanol (8:1), which yielded iDSPE (35.8 mg, 44.2%) as navy blue solid. The product, iDSPE was subsequently characterized by thin layer ninhydrin assay (TCL, DCM: MeOH = 8: 1, $R_f$ = 0.3). It was shown that the blue spots on the left column represent the unreacted ir623-NHS (top spot) and product iDSPE (bottom spot). The purified iDSPE was characterized by mass spectrometry, (TOF-MS *m*/*z*: 1674.0 [M−H]). Finally, the absorbance and fluorescence spectra of ir623 and iDSPE were recorded on a UV–vis spectrophotometer and a NIR spectral system.

### 2.3. Preparation of iDSPE-embed liposomes (iLPs) with two different sizes

Liposomes were prepared using the previously described thin-film hydration method [10]. Lipid components of the iLPs were HSPC, cholesterol, PEG-DSPE, and iDSPE at molar ratios of 100:10:5:0.1 with a mass of total lipids weighing approximately 20 mg. Formulation components were weighed into a 50 mL round bottom flask and dissolved in ~5 mL chloroform/methanol (4:1). Then the solvent was evaporated using rotary evaporator at 40◦C in order to form a uniform lipid thin film, and an in-house vacuum was used to remove the residual solvent. When solvents were completely removed, the lipid film was hydrated with phosphate-buffered saline (PBS, pH 7.4) at 65◦C for 60 min. Next, the resulting vesicle suspension was extruded through polycarbonate filters (Avanti Polar Lipids, Alabaster, AL, USA) of 200 nm and 100 nm (five times each) for iLPs-1. The resulting vesicle suspension was extruded through polycarbonate filters of 400 nm (five times) for iLPs-2.

### 2.4. Characterization of iLPs

The size, surface potential and size distribution of iLPs were measured at 25 ± 0.1 °C by DLS detector Malvern Zetasizer and TEM. The TEM samples were prepared by placing a drip of iLPs onto 300-mesh copper-grid, and a drip of 3 wt% phosphotungstic acid was dropped on the sample for negative staining, then keep the sample at room temperature overnight for drying.

### 2.5. Optical property and stability of iLPs

Absorption spectra were obtained using a UV–vis spectrophotometer at room temperature and in the spectral range of 600–900 nm. Probe ir623 (1 mL, 1 μM) and iDSPE (1 mL, 1 μM) were studied by absorption spectroscopy in methanol or chloroform. Fluorescence Spectra were determined using the spectrofluorometer. Probe ir623 (1 mL, 1 μM) and iDSPE (1 mL, 1 μM) were separately added into the 1 mL color comparison tubes and studied by fluorescence spectroscopy in PBS, methanol solutions or serum.

The optical stability of ir623, iLPs-1 and iLPs-2 in serum were determined by the method reported previously using a fluorescence spectroscopy [19]. To evaluate stability in serum, 10 μM ir623, iLPs-1 and iLPs-2 was incubated in 100% fetal bovine serum at 37 °C for 1, 2, 4, 8, 22, 28 and 48 h. Fluorescence intensities were detected in 10 mL color comparison tubes. Fluorescence intensities were detected by Cary Eclipse spectrofluorometer (623 nm excitation, 600–800 nm emission). All experiments were carried out in triplicates and data was plotted as the mean values ± standard deviation (SD). Lastly, the physical stability of iLPs was further evaluated for any size change during storage at 4 °C for 3 weeks.

### 2.6. Cell lines and cell culture

Human colon adenocarcinoma cells (HT-29) were used in this study provided by Cell Bank of Shanghai Institute of Cell Biology, Chinese Academy of Sciences. Human colon adenocarcinoma cells (HT29) were maintained in McCoy's 5A (modified) medium, respectively, supplemented with 10% FBS and 1% penicillin/streptomycin. Cells were cultured in 25 $cm^2$ sterile tissue culture flask at 37 °C and 5% $CO_2$ level. Cells were passaged twice a week using trypsin-EDTA when reaching 80% confluency.

### 2.7. Cell viability assay

The CCK-8 assays were conducted to assess the biocompatibility of ir623 and iLPs to HT29. Briefly, 5000 cells per well were seeded in 96-well plates in 100 μL of complete culture medium (containing 10% fetal bovine serum) and incubated at 37 °C in a $CO_2$ incubator for 24 h. Then the volume in each well was replaced with 100 μL of blank, ir623, iLPs-1 or iLPs-2. Varied ir623, iLPs-1 and iLPs-2 concentrations 2.5, 5, 10, 15, 20 μM were tested. At the end of the incubation period, 10 μL of CCK-8 reagent (Beyotime, Shanghai, China) was added to the cells and further incubated for 2 h. Afterward the 96-well plate was analyzed at a 450 nm wavelength in an Infinite 200 PRO plate reader (Tecan, Switzerland) to determine cell viability. Media without test material was used as control.

### 2.8. In vitro cellular uptake

$2 \times 10^4$ HT29 cells were seeded into 6-well chambered coverglasses in 1 mL of medium. After 24 h culturing at 37 °C under a circumstance containing 5% $CO_2$, the medium was replaced by new medium with 20 μL of two types of iLPs. After 4 h incubation, the cells were washed for thrice and fixed with PBS. Finally, the cells were observed by confocal laser scanning microscope.

### 2.9. Animals and tumor model

The animal experiments were carried out according to the protocol approved by the Ministry of Health in People's Republic of China (document no. 55, 2001) and the guidelines for the care and use of Laboratory Animals of China Pharmaceutical University. Female BALB/C nude mice (20 ± 2 g, 6–8 weeks old) were purchased from Nanjing model animal research institute (Nanjing, China) and received care under standard housing conditions. HT-29 cells ($6 \times 10^6$/100 μL PBS) were administered by subcutaneous injection into the flank region of the mice. 2 weeks after post-inoculation, the xenograft tumor model was built. Tumor volume was calculated as (tumor length) × (tumor width) $^2$/2.

### 2.10. In vivo NIR molecular imaging and biodistribution

The imaging studies were performed when tumor volumes of mice reached about 100 $mm^3$. The tumor-bearing mice were randomly divided into three groups (n = 3) and intravenously injected with ir623, iLPs-1 or iLPs-2, respectively. The equivalent ir623 dose was kept at 0.5 mg/kg. The NIR images of mice were obtained at 0.5, 2, 4, 8, 24 and 48 h postinjection using the ex/in vivo imaging system with a 630 nm excitation wavelength and 710 nm filter. After imaging, the mice were immediately sacrificed and organs including heart, liver, spleen, kidney, intestine and tumors were harvested for the ex vivo imaging under the same conditions as described above.

### 2.11. Statistical analysis

All values shown are in mean ± SD unless otherwise indicated. ANOVA was used for statistical analysis by SPSS software. The differences were considered to be significant for $^*P < 0.05$, and to be very significant for $^{**}P < 0.01$.

## 3. Results and discussion

### 3.1. Synthesis and characterization of iDSPE

Fig. 1 shows the chemical structure of ir623 and iDSPE. As shown in Fig. 1, the ir623 was synthesized by a three-step reaction followed the conventional processes for synthesis of ICG and other ICG derivatives reported elsewhere [26–28]. Subsequently, DSPE-ir623 (iDSPE) was synthesized by a three-step reaction as shown in Fig. 1. TLC, MS spectra and FT-IR spectroscopy were shown in Figs. S1 and S2 . Analysis of the data showed that iDSPE was successfully prepared. In this study, one molecule of ir623

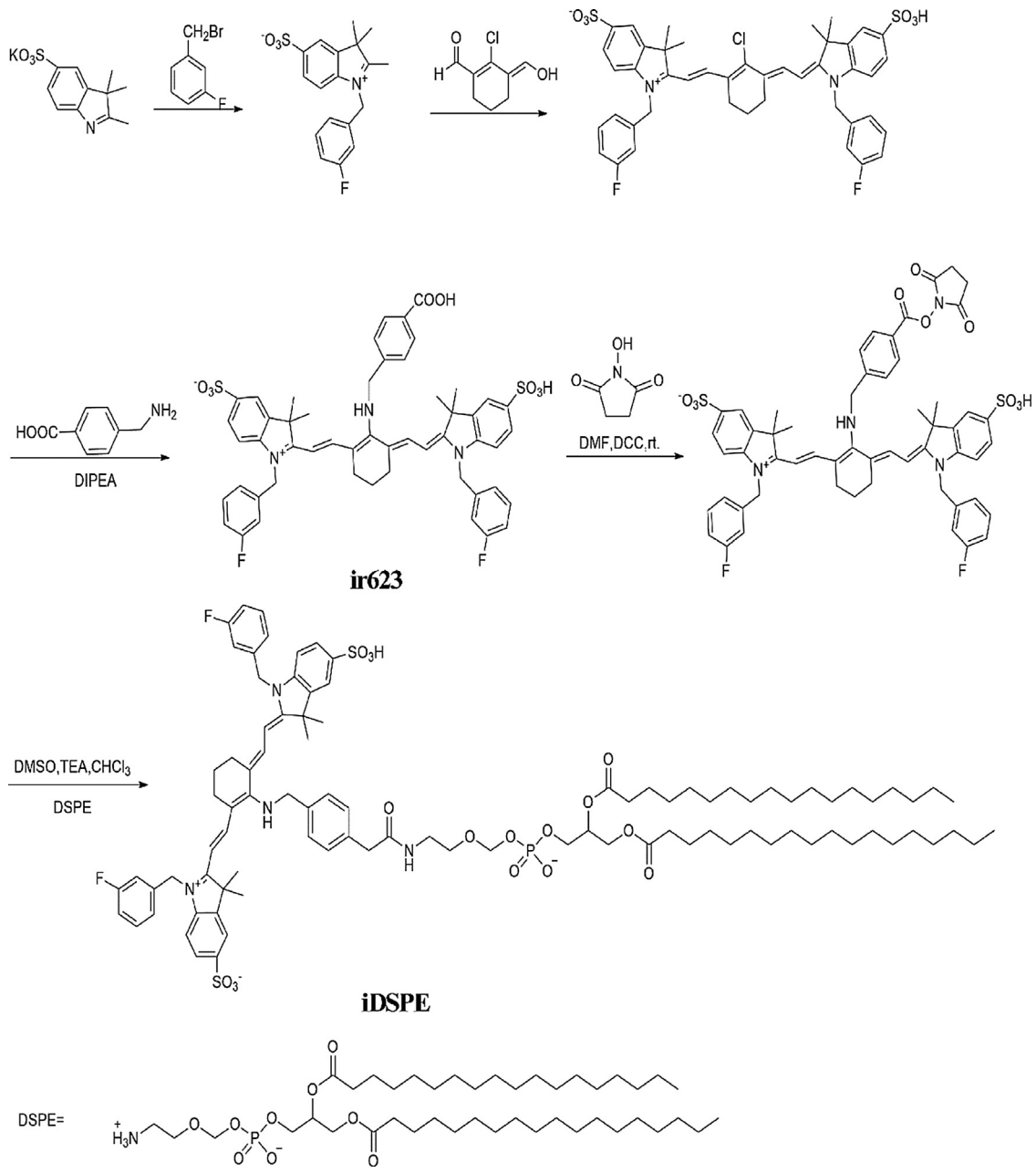


**Fig. 1.** Schemes of chemical synthesis procedure of DSPE-ir623 (iDSPE).

was conjugated with one molecule of 1, 2-distearoyl-sn-glycero-3-phosphoethanolamine (DSPE) by controlling the reactants ratio and reaction conditions.

### 3.2. Optical properties and stability of ir623 and iDSPE

To analyze the optical properties of ir623 and iDSPE, we detected their absorption and emission spectrum in $CH_3OH$ and $CHCl_3$ (Fig. 2). The colors of the $CH_3OH$ and $CHCl_3$ solutions of iDSPE were intense blue similar to ir623. The absorption and emission peaks of ir623 and iDSPE in different media ($CH_3OH$ and $CHCl_3$) were in NIR region (600–900 nm). $\lambda_{max}$ of excitation and emission of ir623 lied in 623/731 nm in $CH_3OH$ and 633/716 nm in $CHCl_3$ respectively. Moreover, $\lambda_{max}$ of excitation and emission of iDSPE lied in 630/710 nm in $CH_3OH$ and $CHCl_3$, which also exhibits a strong blue excitation peak and a large Stokes shifts more than 25 nm with highly fluorescent (Table 1). Most of the polymethine cyanine dyes have the fatal disadvantage of their Stokes shifts being less than 25 nm. A small Stokes shift could result in self-quenching and measurement error by excitation and scattering light [29]. It is obvious that ir623 and iDSPE with a larger Stokes shift would have promising applications in fluorescent bioassays.

**Table 1**
Absorptions, emissions, and molar absorption coefficients of iDSPE and ir623.

| | Solvent | $\lambda_{max}$, abs (nm) | $\lambda_{max}$, em (nm) | Stokes shift (nm) |
|---|---|---|---|---|
| ir623 | $CH_3OH$ | 623 | 731 | 108 |
| | $CHCl_3$ | 633 | 716 | 83 |
| iDSPE | $CH_3OH$ | 630 | 710 | 80 |
| | $CHCl_3$ | 630 | 710 | 80 |

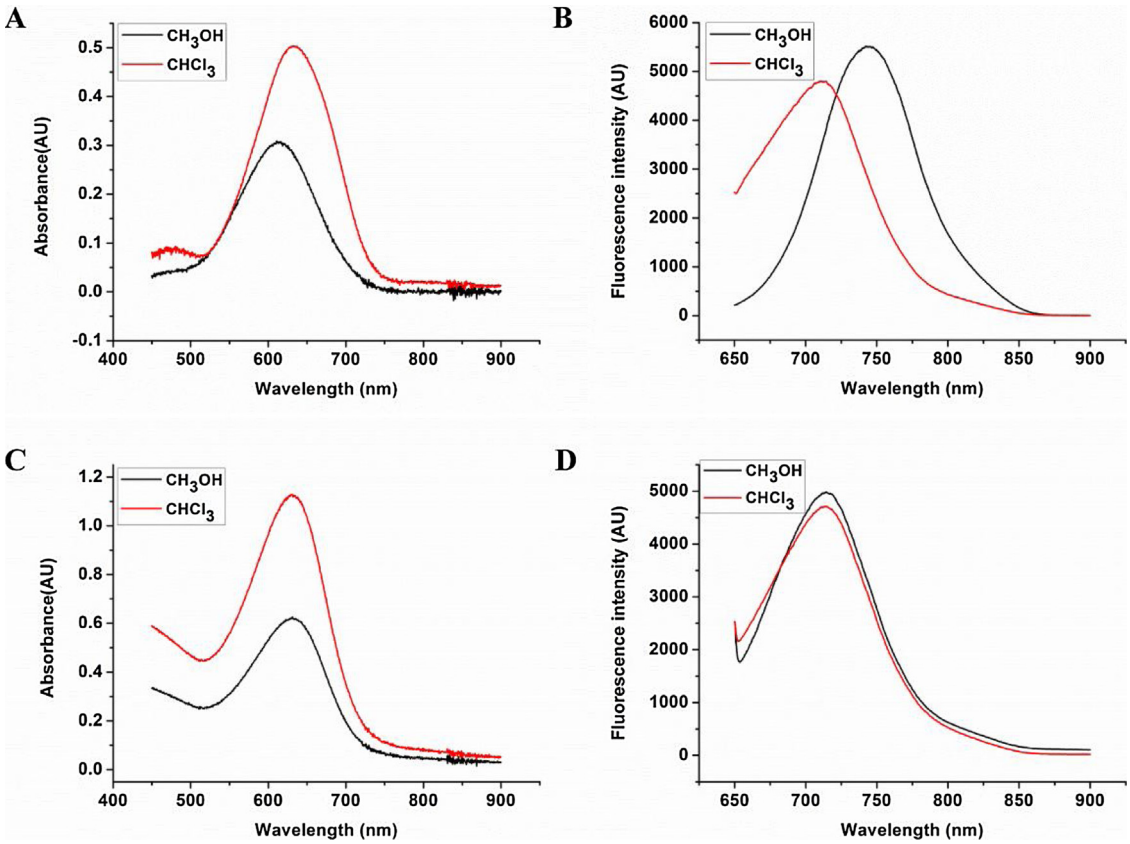


**Fig. 2.** The absorption and fluorescence spectral property of ir623 and iDSPE were examined in methanol solutions or chloroform solutions. A and B: The absorption and emission spectra of ir623 (1 μM) in methanol ($CH_3OH$) and chloroform ($CHCl_3$). C and D: The absorption and emission spectra of iDSPE (1 μM) in methanol ($CH_3OH$) and chloroform ($CHCl_3$).

### 3.3. Formulation and characterization of liposomes (LPs) consisting of iDSPE

As represented in Table 2, to investigate the applications of iDSPE, we developed liposomes (LPs) consisting of iDSPE with two different hydrodynamic sizes of ~100 nm (iLPs-1) and ~400 nm (iLP-2). Afterward, we systematically evaluated the physiochemical characters of iLPs. Diameter and surface potential of two iLPs were measured by dynamic light scattering (DLS) (Fig. 3A and B). The average size of two iLPs in water was 105.31 ± 0.43 nm and 373.97 ± 0.61 nm respectively, and average zeta potential were −26.31 ± 5.74 mV and −23.56 ± 3.15 mV iDSPE-free liposomes with the same composition were prepared using the same method as iLPs-1. The average size of the iDSPE-free liposomes was 109.48 ± 0.85 nm, which was similar to iLPs-1. When blending with liposomal compositions, the iDSPE molecules were expected to be inserted into the lipid bilayers of the liposomal structures. Transmission electron microscopy (TEM) was also utilized to investigate the morphology of iLPs. The images obviously demonstrated that iLPs were divided into two types of distribution and each type of iLPs exhibited an excellent monodispersity and the formation of spherical nanostructures (Fig. 3C and D).

The size stability study by DLS indicated the diameter of iLPs-1 and iLPs-2 remained their size without evident variation after 3 weeks (Fig. 3E). Fluorescence intensity (FL) of free ir623 and two types of iLPs was also detected by fluorescence spectroscopy for 48 h in serum to evaluate the fluorescence stability of ir623. Unlike the free ir623 with the rapid decrease of fluorescence intensity, iLPs still remained 83.33% of the initial fluorescence intensity after 48 h (Fig. 3F). Obviously, the fluorescence stability of ir623 was significantly improved when they were chemically conjugated with DSPE (iDSPE) entrapped by PEGylated liposomes. Free heptamethine dye in aqueous solution would aggregate to form dimers, resulting in fluorescence selfquenching. However, it is reasonable for the improvement of fluorescence stability of iLPs when the iDSPE molecules were inserted into the lipid bilayers of the liposomal structures to prevent aggregation of ir623.

Particle size and zeta potential were measured in PBS buffer (70 mM NaCl, pH 7.4). Data are presented as mean ± standard deviation (S.D.) (n = 3).

### 3.4. Cytotoxicity evaluation

Biocompatibility assessments of ir623 and iLPs were conducted by determining the cytotoxicity to HT29 cells. Cytotoxicity was measured using the CCK-8 assay, to quantify living HT29 cells in the wells after incubation with ir623 and iLPs. The results are displayed in Fig. 4. The cytotoxicity assay showed that ir623 and iLPs

**Table 2**
Composition and physical properties of various iDSPE-embeded liposomes (iLPs).

| iDSPE-embeded liposomes (iLPs) | Composition with the molar ratio | Size (nm) (PDI) | Zeta potential (mV) |
|---|---|---|---|
| iLPs-1 | HSPC:CHOL:PEG-DSPE:iDSPE = 100:10:5:0.1 | 105.31 ± 0.43 (0.152 ± 0.02) | −26.31 ± 5.74 |
| iLPs-2 | HSPC:CHOL:PEG-DSPE:iDSPE = 100:10:5:0.1 | 373.97 ± 0.61 (0.187 ± 0.03) | −23.56 ± 3.15 |

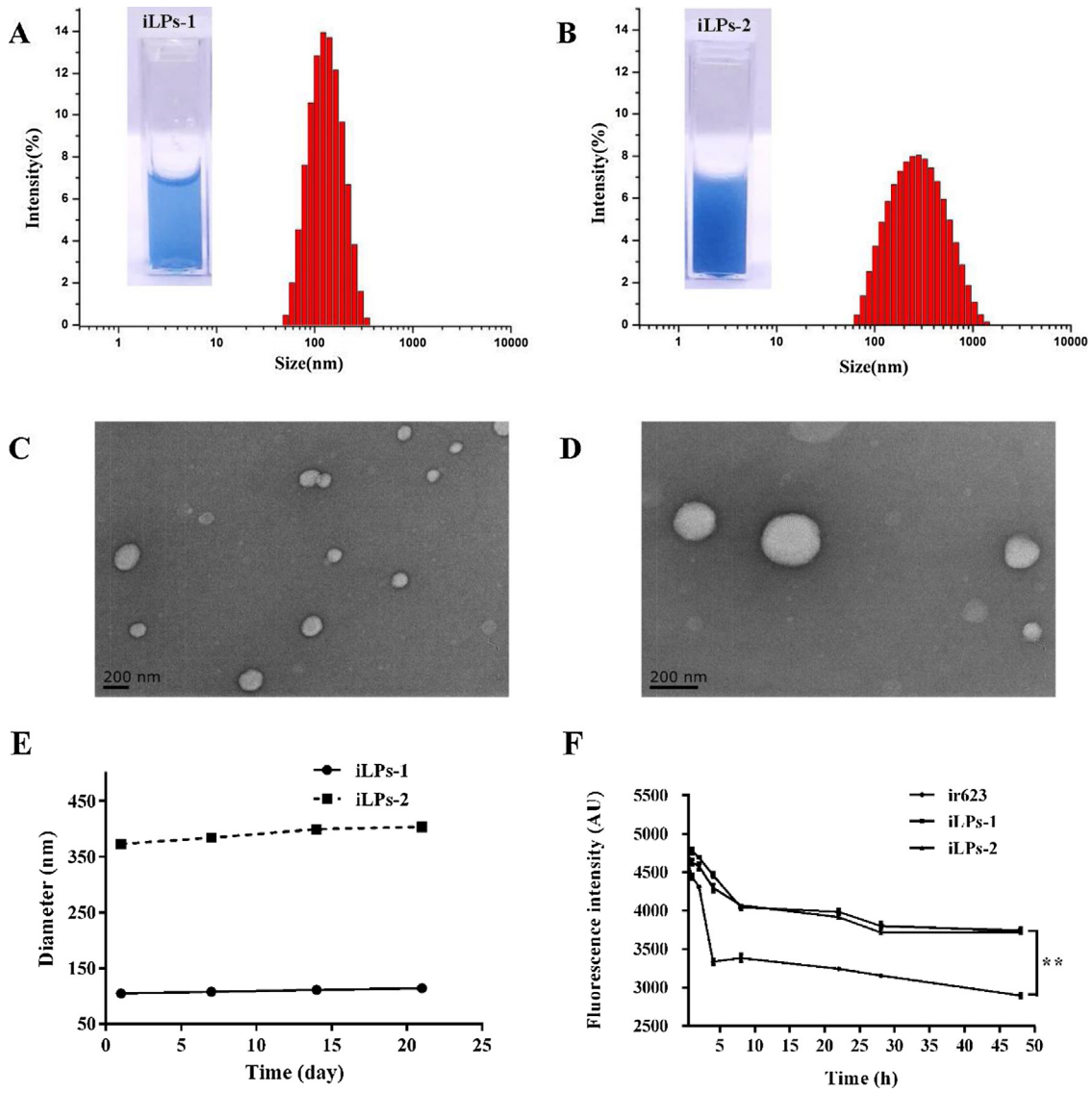


**Fig. 3.** Characterization and physical stability of iLPs. A and B: Particle size distribution and photograph of iLPs-1 and iLPs-2. C and D: TEM image of iLPs-1 and iLPs-2. E: size changes of iLPs were examined as a function of time at 4 °C for 3 weeks. F: Optical stability of iLPs in serum were determined.

displayed very low toxicity to HT29 cells. After treatment with ir623 and iLPs, cell viabilities were more than 91.2% at 24 h (Fig. 4A) and over 85.5% at 48 h (Fig. 4B) at various concentrations. Furthermore, no obvious negative effect was observed on HT29 cells. These results suggested that iDSPE is a safe and low toxicity probe and can be used for nanostructured lipid carriers. In the new fluorescence probe, ir623 is a derivative of ICG, approved by FDA for human application. As a conjugation of lipid, the final product was purified and the organic solvent used in synthesis was completely removed. That is the reason that ir623 and iLPs showed nearly no cytotoxic-

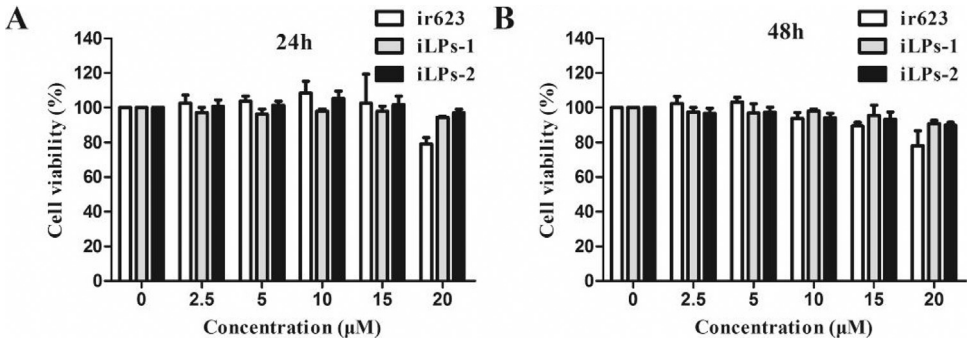


**Fig. 4.** The viability of HT29 cells cultured with ir623 and iLPs in comparison with ir623 at the same dose incubated for 24 h and 48 h. Data were presented as the mean cell viability with standard deviation after triplicate analysis. P value <0.05 is indicated by one asterisk (*).

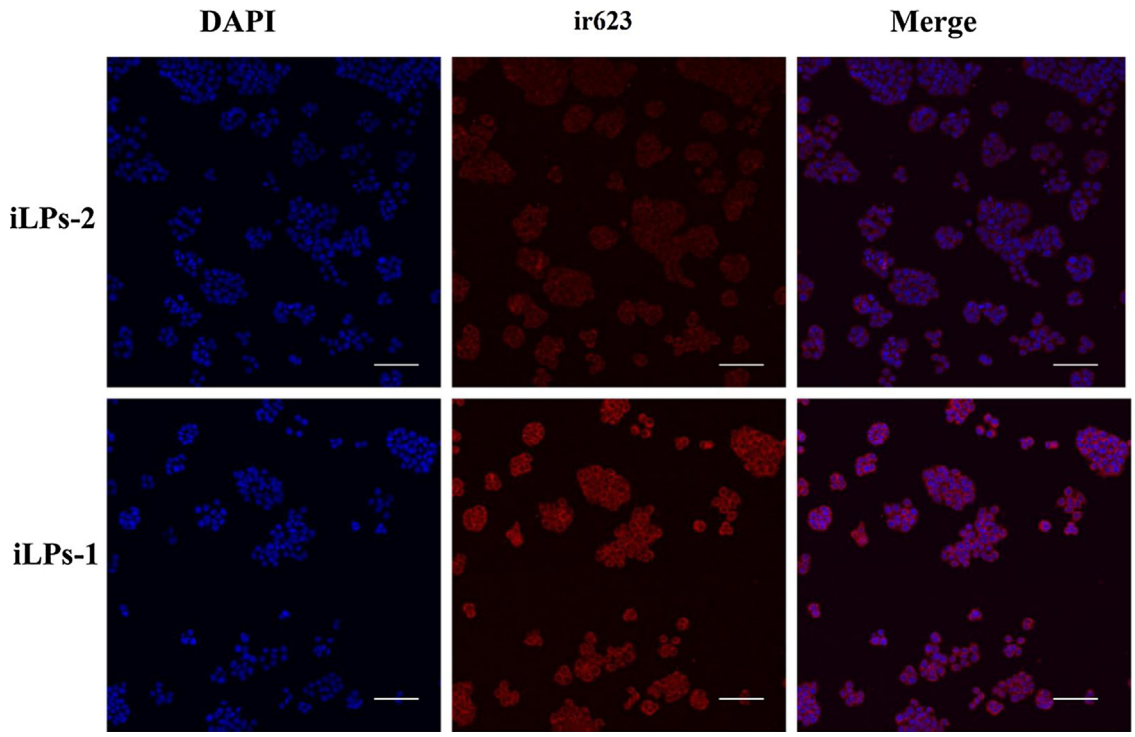


**Fig. 5.** Confocal fluorescence images after 4 h incubation with iLPs-1or iLPs-2. Blue represents the fluorescence of DAPI and red represents the fluorescence of ir623 (scale bar, 50 μm). (For interpretation of the references to colour in this figure legend, the reader is referred to the web version of this article.)

ity in MTT assay. And the non-cytotoxicity of the probe makes it a potential agent for clinical application.

To assess the effect of surface modification on the hemocompatibility of iLPs, hemolytic effect of samples to RBCs was investigated. The data was shown in Fig. S3.

### 3.5. *In vitro cell imaging and cellular uptake*

Based on the optical properties of ir623, the cellular uptake behaviors of liposomes depending on particle size were evaluated in HT29 cells by confocal microscopy. After 4 h incubation, the DAPI stained nucleus (blue) surrounded by ir623 (red) was observed in of all the particles irrespective of particle size, suggesting the successful internalization of iLPs into the cytoplasm by HT29 cells. Higher NIR fluorescence signals could be observed in iLPs-1 group cells, illustrating that ir623 could efficiently distribute into cells via iLPs-1 transportation. The fluorescence signals in iLPs-2 group cells was not that sharp compared to iLPs-1 group, displaying a less ir623 distribution into cells (Fig. 5). It had been proved that the size of nanoparticles always plays a key role in their adhesion to and interaction with the biological cells and ~100 nm sized particles were taken up efficiently for nanostructured lipid carriers (NLC) [30]. Therefore, iLPs-1 could be most internalized by cells and the highest amount of ir623 could accumulate in cells in iLPs-1 group. And it was obvious to conclude that the size of iLPs had a significant effect on delivering drugs into HT29 cells.

### 3.6. *In vivo NIR-fluorescence imaging and biodistribution analysis*

To examine iDSPE for use in NIR-imaging in vivo, various formulations were injected into tumor-bearing mice via tail intravenous injection. The results for real-time imaging and biodistribution of ir623 and the two different iLPs were observed in HT-29 tumor bearing mice by ex/in vivo imaging system (Fig. 6A). In the case of free ir623 treated mice, strong fluorescence signals were observed in living body after administration of free ir623. However, free ir623 solution showed nonspecific distribution of fluorescence all over the body within 2 h, with rapidly decreased fluorescence signals at 12 h postinjection and almost disappeared after 48 h postinjection (Fig. 6B). In comparison with ir623, the results demonstrated that two types of iLPs could be reserved in living body for a longer time. Obviously, an active accumulation of fluorescence intensity was clearly observed in the tumor at 4 h post-injection for the mice receiving iLPs-1 and reached the maximum fluorescence intensity at about 8 h. The iLPs-1 treated mice exhibited detectable NIR fluorescence signals at 48 h postinjection. In the meantime, the tumor was distinguishable from other tissues with good fluorescence contrast, showing excellent tumor targeting capability. Although fluorescence intensity was also observed in the mice receiving iLPs-2, high fluorescence signals were observed in liver compared with these receiving iLPs-1 at the same time significantly.

To obtain detailed information about the probe's distribution, the mice were sacrificed and tumor tissue as well as other organs were harvested for the ex vivo fluorescence imaging at 48 h postinjection. As shown in Fig. 6B, weak signals were exhibited in all organs of control mice treated with free ir623. Consistent with the in vivo observation, the accumulation of iLPs-1 in the tumor was much higher than that of iLPs-2 indicating its selectively targeted capability in the tumor site. However, the fluorescence signal showed a long-term existence in liver, and the period was more than 48 h indicating the obvious liver accumulation of the iLPs-2. Moreover, the intestines displayed high fluorescence signal (Shown in Fig. 6B). Since the bright fluorescence signal was also observed in dejecta, it was reasonably concluded that the NIR fluorescence dye was cleared via the hepatobiliary route into the intestine, which was totally the same as ICG [27,31].

In general, smaller nanoparticles with a size of 50–150 nm escape from the phagocytosis of the reticuloendothelial system (RES), promoting a long circulation life time in vivo, demonstrating a greater EPR effect and intratumoral distribution. Larger nanoparticles have more extensive opsonin binding, which results in enhanced uptake via liver phagocytosis, lead to in liver accumula-

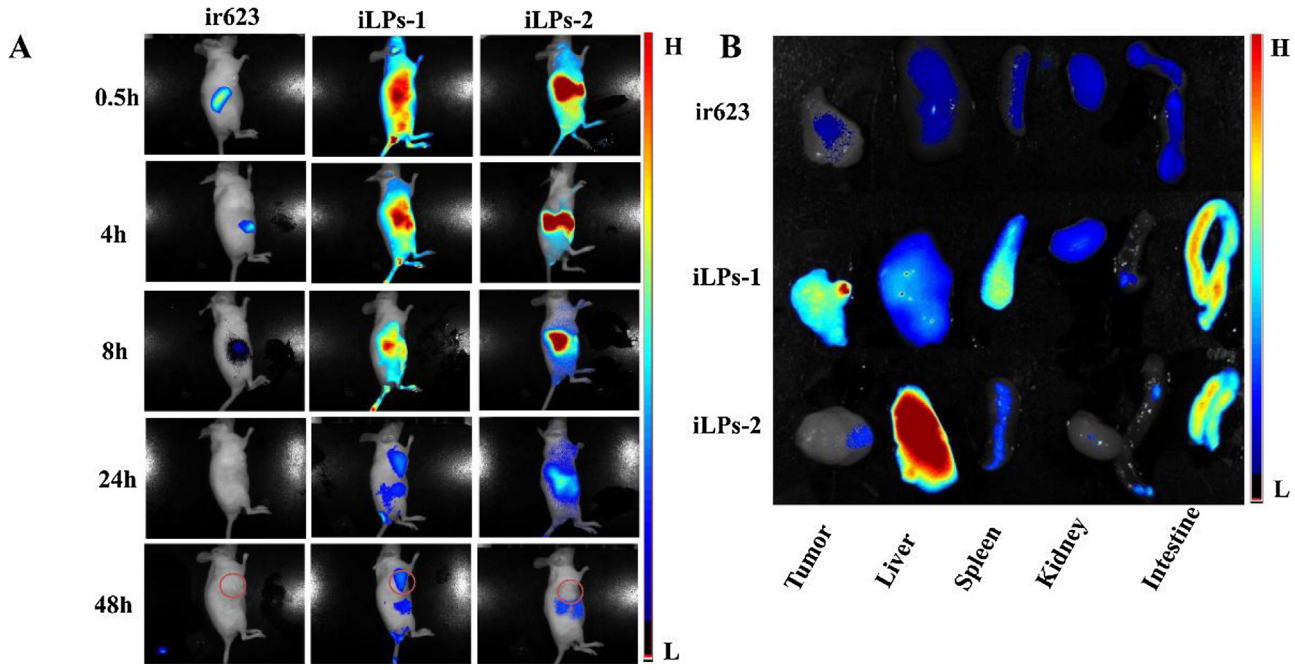


**Fig. 6.** Molecular imaging and biodistribution in vivo. The free ir623, iLPs-1or iLPs-2 were intravenously administrated the HT29 tumor-bearing mice and the tumors and major organs were imaged with the ex/in vivo imaging system. A: Fluorescence signal was obtained in tumor sites at 0.5 h, 4 h, 8 h, 24 h and 48 h after administration of free ir623, iLPs-1or iLPs-2. B: Ex-vivo fluorescence images of major organs and tumors were obtained at 48 h post-injection of free ir623, iLPs-1or iLPs-2.

tion. Therefore, these two different size of iLPs apparently extended ir623 circulation time in living body, exhibited different distribution, and provided a noninvasive and visible method to analyze the biodistribution of NPs in vivo.

## 4. Conclusions

In summary, we successfully developed a novel NIR fluorescence probe iDSPE with high fluorescence, which was conjugated by DSPE and indocyanine green derivative ir623 via covalent bond. Then we fabricated iDSPE-embeded liposomes (iLPs) with two different hydrodynamic sizes (~100 nm and ~400 nm) using thin-film hydration method to demonstrate the size-dependent cellular uptake and in vivo biodistribution of nanoliposomes. Physicochemical properties of iLPs were also verified, such as particle size, morphology. Besides, optical property of iLPs were stable for fluorescence dye labelling, suggesting that the iLPs can represent its original form. Finally, we have demonstrated through a series of in vitro and ex vivo studies of particle size effect on cellular uptake and in vivo biodistribution of nanoliposomes. Our findings confirmed that size could not only obviously influence endocytosis of iLPs, but also affect their biodistribution in vivo. Furthermore, iLPs-1 with smaller size showed much more cell uptake by HT-29 cells and improved accumulation in HT-29 xenograft tumor tissue, while iLPs-2 showed accumulation in the liver and spleen. These results indicated that particle size was a key factor for the regulation of intracellular trafficking and biodistribution of liposomes and provided new insight into the development of more effective lipid based nanoparticles (LBNs). Hence, we offered a novel NIR fluorescence probe iDSPE as an optical tracer for lipid based nanoparticles (LBNs) with low cytotoxicity and good stability. In addition, it also suggested that iDSPE might be a promising tool for the reliable tracing of LBNs. It can be good models for studies comprehending the accurate identification of LBNs in vivo and explore the in vivo fate of LBNs.

## Acknowledgements

This research was financially supported by National Natural Science Foundation of China General Program (81671745), and Industry Project of Jiangsu Science-technology Support Plan (BE2013840), Science and Technology Development Program of Suzhou (ZXY201412).

## Appendix A. Supplementary data

Supplementary data associated with this article can be found, in the online version, at https://doi.org/10.1016/j.colsurfb.2017.11.033.

## References

[1] K. Park, Controlled drug delivery systems: past forward and future back, J. Controll. Release Soc. 190 (2014) 3–8.
[2] N. Martinho, Recent advances in drug delivery systems, J. Biomater. Nanobiotechnol. 02 (2011) 510–526.
[3] H. Khodabandehloo, H. Zahednasab, A. Ashrafi Hafez, Nanocarriers usage for drug delivery in cancer therapy, Iran. J. Cancer Prev. 9 (2016) e3966.
[4] S.P. Egusquiaguirre, M. Igartua, R.M. Hernandez, J.L. Pedraz, Nanoparticle delivery systems for cancer therapy: advances in clinical and preclinical research, Clin. Transl. Oncol. 14 (2012) 83–93.
[5] Y.-H. Park, K.A. Min, Y.-K. Song, S. Ham, C.-K. Kim, Chemically conjugated novel liposomal formulation for intravenous delivery of cyclosporin A, Colloids Surf. A: Physicochem. Eng. Aspects 495 (2016) 229–237.
[6] T.M. Allen, P.R. Cullis, Liposomal drug delivery systems: from concept to clinical applications, Adv. Drug Deliv. Rev. 65 (2013) 36–48.
[7] S. Jain, N. Patel, M.K. Shah, P. Khatri, N. Vora, Recent advances in lipid-based vesicles and particulate carriers for topical and transdermal application, J. Pharm. Sci. 106 (2017) 423–445.
[8] N. Akhtar, R.A. Khan, Liposomal systems as viable drug delivery technology for skin cancer sites with an outlook on lipid-based delivery vehicles and diagnostic imaging inputs for skin conditions', Prog. Lipid Res. 64 (2016) 192–230.
[9] S. Fang, Y. Niu, W. Zhu, Y. Zhang, L. Yu, L. Yu, Liposomes assembled from a dual drug-tailed phospholipid for cancer therapy, Chem. Asian J. 10 (2015) 1232–1238.
[10] F. Yan, H. Wu, H. Liu, Z. Deng, H. Liu, W. Duan, X. Liu, H. Zheng, Molecular imaging-guided photothermal/photodynamic therapy against tumor by

iRGD-modified indocyanine green nanoparticles, J. Controll. Release Soc. 224 (2016) 217–228.
[11] A. Suganami, Y. Iwadate, S. Shibata, M. Yamashita, T. Tanaka, N. Shinozaki, I. Aoki, N. Saeki, H. Shirasawa, Y. Okamoto, Y. Tamura, Liposomally formulated phospholipid-conjugated indocyanine green for intra-operative brain tumor detection and resection, Int. J. Pharm. 496 (2015) 401–406.
[12] M. Gaber, W. Medhat, M. Hany, N. Saher, J.Y. Fang, A. Elzoghby, Protein-lipid nanohybrids as emerging platforms for drug and gene delivery: challenges and outcomes, J. Controll. Release Soc. 254 (2017) 75–91.
[13] J. Qi, J. Zhuang, Y. Lu, X. Dong, W. Zhao, W. Wu, In vivo fate of lipid-based nanoparticles, Drug Discovery Today 22 (2017) 166–172.
[14] M. Zhang, R. Charles, H. Tong, L. Zhang, M. Patel, F. Wang, M.J. Rames, A. Ren, K.A. Rye, X. Qiu, D.G. Johns, M.A. Charles, G. Ren, HDL surface lipids mediate CETP binding as revealed by electron microscopy and molecular dynamics simulation, Sci. Rep. 5 (2015) 8741.
[15] L. Azhar Shekoufeh Bahari, H. Hamishehkar, The impact of variables on particle size of solid lipid nanoparticles and nanostructured lipid carriers; a comparative literature review, Adv. Pharm. Bull. 6 (2016) 143–151.
[16] J. Chen, H. Chen, S. Cui, B. Xue, J. Tian, S. Achilefu, Y. Gu, Glucosamine derivative modified nanostructured lipid carriers for targeted tumor delivery, J. Mater. Chem. 22 (2012) 5770.
[17] H. Yuan, C.Y. Chen, G.H. Chai, Y.Z. Du, F.Q. Hu, Improved transport and absorption through gastrointestinal tract by PEGylated solid lipid nanoparticles, Mol. Pharm. 10 (2013) 1865–1873.
[18] L. Li, X. An, X. Yan, Folate-polydiacetylene-liposome for tumor targeted drug delivery and fluorescent tracing, Colloids Surf. B: Biointerfaces 134 (2015) 235–239.
[19] T. Toyota, H. Fujito, A. Suganami, T. Ouchi, A. Ooishi, A. Aoki, K. Onoue, Y. Muraki, T. Madono, M. Fujinami, Y. Tamura, H. Hayashi, Near-infrared-fluorescence imaging of lymph nodes by using liposomally formulated indocyanine green derivatives, Bioorg. Med. Chem. 22 (2014) 721–727.
[20] K.M. Kim, M.K. Kim, H.J. Paek, S.J. Choi, J.M. Oh, Stable fluorescence conjugation of ZnO nanoparticles and their size dependent cellular uptake, Colloids Surf. B: Biointerfaces 145 (2016) 870–877.
[21] C. Vitorino, F.A. Carvalho, A.J. Almeida, J.J. Sousa, A.A. Pais, The size of solid lipid nanoparticles: an interpretation from experimental design, Colloids Surf. B: Biointerfaces 84 (2011) 117–130.
[22] J.S. Choi, J. Cao, M. Naeem, J. Noh, N. Hasan, H.K. Choi, J.W. Yoo, Size-controlled biodegradable nanoparticles: preparation and size-dependent cellular uptake and tumor cell growth inhibition, ColloidsS urf. B Biointerfaces 122 (2014) 545–551.
[23] H. Cabral, Y. Matsumoto, K. Mizuno, Q. Chen, M. Murakami, M. Kimura, Y. Terada, M.R. Kano, K. Miyazono, M. Uesaka, N. Nishiyama, K. Kataoka, Accumulation of sub-100 nm polymeric micelles in poorly permeable tumours depends on size, Nat. Nanotechnol. 6 (2011) 815–823.
[24] P. Zhao, M. Zheng, C. Yue, Z. Luo, P. Gong, G. Gao, Z. Sheng, C. Zheng, L. Cai, Improving drug accumulation and photothermal efficacy in tumor depending on size of ICG loaded lipid-polymer nanoparticles, Biomaterials 35 (2014) 6037–6046.
[25] Q.P. Su, W. Du, Q. Ji, B. Xue, D. Jiang, Y. Zhu, J. Lou, L. Yu, Y. Sun, Vesicle size regulates nanotube formation in the cell, Sci. Rep. 6 (2016) 24002.
[26] A. Suganami, T. Toyota, S. Okazaki, K. Saito, K. Miyamoto, Y. Akutsu, H. Kawahira, A. Aoki, Y. Muraki, T. Madono, H. Hayashi, H. Matsubara, T. Omatsu, H. Shirasawa, Y. Tamura, Preparation and characterization of phospholipid-conjugated indocyanine green as a near-infrared probe, Bioorg. Med. Chem. Lett. 22 (2012) 7481–7485.
[27] D.M. Mahounga, L. Shan, C. Jie, C. Du, S. Wan, Y. Gu, Synthesis of a novel L-methyl-methionine-ICG-Der-02 fluorescent probe for in vivo near infrared imaging of tumors, Mol. Imaging Biol. 14 (2012) 699–707.
[28] H.S. Choi, K. Nasr, S. Alyabyev, D. Feith, J.H. Lee, S.H. Kim, Y. Ashitate, H. Hyun, G. Patonay, L. Strekowski, M. Henary, J.V. Frangioni, Synthesis and in vivo fate of zwitterionic near-infrared fluorophores, Angew. Chem. 50 (2011) 6258–6263.
[29] C. Sun, J. Cai, J. Chen, Y. Wu, P. Wang, G. Zhou, X. Zong, B. Chen, Y. Lv, M. Ji, The synthesis of a novel near-infrared fluorescent probe and its application in imaging of living cells, Appl. Biochem. Biotechnol. 175 (2014) 1644–1650.
[30] S. Zhang, J. Li, G. Lykotrafitis, G. Bao, S. Suresh, Size-dependent endocytosis of nanoparticles, Adv. Mater. 21 (2009) 419–424.
[31] X. Tan, S. Luo, D. Wang, Y. Su, T. Cheng, C. Shi, A NIR heptamethine dye with intrinsic cancer targeting, imaging and photosensitizing properties, Biomaterials 33 (2012) 2230–2239.